Electrical Engineering (2026) 108:94
https://doi.org/10.1007/s00202-025-03387-y

ORIGINAL PAPER

Probing armour losses formulae from CIGRE technical Brochure 908

Pasquale Cambareri[1] · Luca Di Rienzo[1] · Carlo de Falco[2] · Massimo Bechis[3]

Received: 28 March 2025 / Accepted: 22 September 2025

Abstract
This paper probes the validity up to 15 kHz of the analytical formulae published in the CIGRE Technical Brochure 908 related to the calculation of the armour losses in single-armoured AC cables, which have been tested in the Brochure at 50 Hz only. After briefly reviewing the theoretical background and carefully explaining the approximations performed by the Brochure, it is shown that for a typical cable, the analytical formulae are reasonably accurate in the estimation of losses up to 15 kHz, but the absolute error increases linearly with frequency.

Keywords Submarine cables · Eddy currents · Ohmic losses · Magnetic losses

1 Introduction

Large armoured three-core cables are typically used to connect Offshore Wind Farms (OWF) to land distribution grids when the distance of the OWF form shore is limited to a few dozen kilometres. The CIGRE Technical Brochure 908 [1] proposes an improvement on the formulae published in the IEC Standard 60287-1-1 [2] for calculating power losses in single-armoured tripolar AC cables. The formulae in the technical brochure (TB) compute the losses in each component of the cable: the phase conductors, the sheaths, and the armour. This paper focuses on the latter, i.e. the armour.

The TB presents two methodologies for calculating the armour losses: *Method 1* builds on the work of Hatlo et al. [3, 4], while *Method 2* relies on the work of Goddard et al. [5]. This paper covers the first method. In [1], care is given to the mathematical calculations, but the fundamental approximations and their implications are not thoroughly discussed. The recent work in [4] expanded on this by presenting the full derivation of the formulae, starting from first principles, and stating the performed mathematical approximations.

After providing the necessary background, and rediscussing the physical significance of the approximations made by the TB in Sect. 3, this paper aims at extending the pool of tests performed by the TB to probe the validity of the formulae beyond 50 Hz, as done by the TB, up to 15 kHz: this is the typical frequency range of interest when considering high-order harmonics introduced by power converters [6]. The computation of eddy current and magnetic losses is aimed at calculating per-unit-length series impedances required by electromagnetic transient simulations.

The formulae are compared to two different numerical methods: one based on finite elements (calculations were carried via a commercial software [7]), and the other with a numerical formulation based on the method of moments [8–10]. It has been observed that the analytical formulae yield reasonably accurate results, but they commit an error that increases linearly with frequency. Analytical formulas are characterized by a negligible computational time, while that of numerical models is typically high. A detailed comparison between computational times of FEM and the method of moments can be found in [9].

Since the scope of this paper is to probe the validity of the TB formulae against numerical methods, the same hypothesis of the TB is assumed: the problem is purely electromagnetic, not coupled with any thermal modelling. The temperature dependence of the material parameters is considered when fixing their values.

✉ Luca Di Rienzo
luca.dirienzo@polimi.it

Carlo de Falco
carlo.defalco@polimi.it

Massimo Bechis
massimo.bechis@prysmian.com

[1] Dipartimento di Elettronica, Informazione e Bioingegneria, Politecnico di Milano, P.zza L. da Vinci, 32, Milano 20133, Italy

[2] MOX, Dipartimento di Matematica, Politecnico di Milano, P.zza L. da Vinci, 32, Milano 610101, Italy

[3] Prysmian Group S.p.A., Via Chiese, 6, Milano 20126, Italy

Published online: 09 January 2026

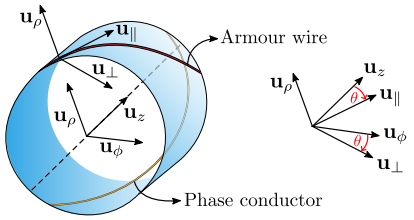

Fig. 1 Global ($\mathbf{u}_\rho$, $\mathbf{u}_\phi$, $\mathbf{u}_z$) and local ($\mathbf{u}_\rho$, $\mathbf{u}_\perp$, $\mathbf{u}_\parallel$) coordinate systems

2 Background

As for the calculation of the armour losses, in the TB the cable is modelled considering the phase conductors and the armour wires. From now on we will refer to them simply as *the conductors* and *the wires*, respectively. Both of them are helically wound around the cable's axis, as shown by Fig. 1. The conductors are assumed to be filamentary. As the focus of this paper is on the formulae for the armour losses, the sheaths will not be taken into account.

The geometric description of the cable relies on two cylindrical coordinate systems, shown in Fig. 1. The *global system* ($\mathbf{u}_\rho$, $\mathbf{u}_\phi$, $\mathbf{u}_z$) is centred on the cable's axis, the *local system* ($\mathbf{u}_\rho$, $\mathbf{u}_\perp$, $\mathbf{u}_\parallel$) follows the helix of a wire. The two systems share the common versor $\mathbf{u}_\rho$, and they are rotated by a fixed angle

$$\theta = \arctan\left(\frac{2\pi r_a}{p_a}\right), \tag{1}$$

where r_a and p_a are the radius and the pitch of the armour's helix. The following rotation matrix operates the conversion *from global to local* coordinates:

$$\mathrm{R}_\theta = \begin{pmatrix} 1 & 0 & 0 \\ 0 & \cos\theta & -\sin\theta \\ 0 & \sin\theta & \cos\theta \end{pmatrix}. \tag{2}$$

Power losses in the armour can be calculated as [11]

$$\Delta S = \frac{j\omega}{2}\int_{V_a}\left(\mathbf{B}\cdot\mathbf{H}_0^* - \mathbf{H}\cdot\mathbf{B}_0^*\right)\mathrm{d}v, \tag{3}$$

where $\mathbf{B}_0$ and $\mathbf{H}_0$ are the induction and magnetic fields in the absence of the armour, $\mathbf{B}$ and $\mathbf{H}$ are the same fields in presence of the armour, the asterisk denotes the complex conjugate, V_a is the volume region of the entire armour, and ω is the angular frequency. It should be observed that the above equation is given in [11] as a relationship that applies strictly speaking to nonconductive materials. Its validity in the time-harmonic regime, that would allow for a complex magnetic susceptibility (or permeability) that includes the conductive effects, is demonstrated in Appendix A. Please note that (3) calculates the total losses in the armour so that $\Re\{\Delta S\}$ is the total active loss which includes both the resistive and the hysteresis losses.

The constitutive relationships are

$$\mathbf{B}_0 = \mu_0\mathbf{H}_0, \quad \mathbf{B} = \mu_0(1+\chi_m)\mathbf{H}, \tag{4}$$

where μ_0 is the vacuum permeability and χ_m is the magnetic susceptibility of the wires. Using (4), the integrand in (3) becomes

$$\mathbf{B}\cdot\mathbf{H}_0^* - \mathbf{H}\cdot\mathbf{B}_0^* = \mu_0\chi_m\mathbf{H}\cdot\mathbf{H}_0^* = \mu_0\mathbf{M}\cdot\mathbf{H}_0^*, \tag{5}$$

where

$$\mathbf{M} = \chi_m\mathbf{H} \tag{6}$$

is the magnetization of the wire. After (5), the expression of the power losses becomes

$$\Delta S = \frac{j\omega}{2}\int_{V_a}\mu_0\mathbf{M}\cdot\mathbf{H}_0^*\mathrm{d}v. \tag{7}$$

Field $\mathbf{H}_0$ is generated by the conductors, and its analytical expression was given by Haber [12]. Let $\xi = \rho, \phi, z$ be a coordinate in the global system, then each component of $\mathbf{H}$ is given by the Fourier expansion

$$H_{0_\xi} = \sum_{m=3k+1,\, k\in\mathbb{Z}} H_{0_m}^{\xi}(\rho)\, e^{jm\left(\phi+\frac{2\pi z}{p_c}\right)}, \tag{8}$$

where p_c is the pitch of the conductors' helix. For each component, the series terms are given by [12]

$$H_{0_m}^{z}(\rho) = \frac{3\eta_m r_c}{p_c} I_m'(\eta_m r_c) I_c K_m(\eta_m\rho), \tag{9}$$

$$H_{0_m}^{\phi}(\rho) = \frac{p_c}{2\pi\rho} H_{0_m}^{z}(\rho), \tag{10}$$

$$H_{0_m}^{\rho}(\rho) = \frac{p_c}{j2\pi m}\left(H_{0_m}^{z}\right)'(\rho), \tag{11}$$

where $\eta_m = 2\pi|m/p_c|$, I_m and K_m are the modified Bessel's function of first and second kind, respectively, and $'$ denotes a total derivative.

Field $\mathbf{M}$ could in principle be obtained by solving the following quasi-static problem *in the armour*:

$$\begin{cases} \nabla\times\mathbf{H} = \sigma\mathbf{E}, \\ \nabla\cdot\mathbf{M} = 0, \end{cases} \tag{12}$$

where σ is the conductivity of the wires and $\mathbf{E}$ is the induced electric field. However, in the approach developed by Hatlo et al. [3], the armour is treated as a unique object, whose

effect on the magnetic field is modelled by a susceptibility tensor represented *in the local system* as

$$\chi_m^\ell = \mathrm{diag}(\chi_\rho,\ \chi_\perp,\ \chi_\parallel), \tag{13}$$

where χ_ρ, $\chi_\perp$, and $\chi_\parallel$ are magnetic susceptibilities to be determined. These susceptibilities incorporate the effect of eddy currents on each component of $\mathbf{H}$; hence with (13), problem (12) translates into an equivalent static one:

$$\begin{cases} \nabla \times \mathbf{H} = \mathbf{0}, \\ \nabla \cdot \mathbf{M} = 0. \end{cases} \tag{14}$$

The susceptibility tensor can be also written in the global system via (2) and (13) as

$$\chi_m = R_\theta^{-1} \chi_m^\ell R_\theta = \begin{pmatrix} \chi_\rho & 0 & 0 \\ 0 & \chi_{\phi\phi} & \chi_{\phi z} \\ 0 & \chi_{z\phi} & \chi_{zz} \end{pmatrix}, \tag{15}$$

with $\chi_{\phi\phi} = \chi_\perp \cos^2\theta + \chi_\parallel \sin^2\theta$, $\chi_{\phi z} = \chi_{z\phi} = (\chi_\parallel - \chi_\perp)\sin\theta\cos\theta$, and $\chi_{zz} = \chi_\perp \sin^2\theta + \chi_\parallel \cos^2\theta$. We should note that the TB [1] writes the tensor in (13) in terms of the relative permeabilities $\mu_\rho = 1 + \chi_\rho$, $\mu_\perp = 1 + \chi_\perp$, and $\mu_\parallel = 1 + \chi_\parallel$. Here, we prefer to argue in terms of the susceptibilities and the magnetization, as their use smooths down the discussion.

This section was a succinct introduction to the concepts that serve as a starting point for this work. In the next section, we accurately describe the approximations in [1].

3 Approximations

In a typical cable, the radius of the wires, r_w, is negligible if compared to the radius of the armour's helix, r_a:

$$r_w \ll r_a. \tag{16}$$

This fact motivates the idea, in the TB, of approximating the armour with a hollow cylinder, whose thickness t is defined in such a way that the volume of the cylinder, $V_t = 2\pi r_a t p_a$, matches that of the armour, $V_a = N\pi r_w^2 l_a p_a$ (see Fig. 2):

$$V_t = V_a \ \Leftrightarrow\ t = \frac{N r_w^2 l_a}{2 r_a}, \tag{17}$$

where N is the number of wires and $l_a = \sqrt{1 + (2\pi r_a/p_a)^2}$ is the pitch factor of the armour. It can be verified that (16) implies

$$t \ll r_a. \tag{18}$$

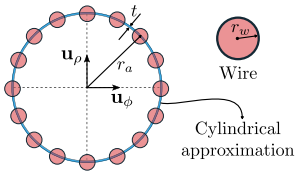

Fig. 2 Cylindrical approximation of the armour

The cylindrical approximation is useful to simplify Gauss' law for $\mathbf{M}$ in (14). In the global system, we have

$$\nabla \cdot \mathbf{M} = \frac{\partial_\rho(\rho M_\rho)}{\rho} + \frac{\partial_\phi M_\phi}{\rho} + \partial_z M_z = 0; \tag{19}$$

however, since this equation holds *in* the cylinder, after (18) we can write $\rho \approx r_a$ and we can *assume in first approximation that* $\partial_\phi M_\phi$ *and* $\partial_z M_z$ *do not vary significantly with* ρ. Equation (19) can then be integrated over the thickness of the cylinder to obtain, after some manipulations,

$$M_\rho\Big|_{r_a+\frac{t}{2}} - M_\rho\Big|_{r_a-\frac{t}{2}} = -\frac{t}{r_a}\partial_\phi M_\phi\Big|_{r_a} - \partial_z M_z\Big|_{r_a}. \tag{20}$$

Equation (20) binds $\mathbf{M}$ on the two sides of the cylinder: it can be translated to an interface condition for $\mathbf{H}$. Indeed, using (15) and (6) we can turn (20) into a constraint on the components of $\mathbf{H}$:

$$\left[H_\rho\Big|_{r_a+\frac{t}{2}} - H_\rho\Big|_{r_a-\frac{t}{2}}\right] = -\frac{t}{r_a}\partial_\phi(\chi_{\phi\phi}H_\phi + \chi_{\phi z}H_z) - \partial_z(\chi_{z\phi}H_\phi + \chi_{zz}M_z). \tag{21}$$

Considering (18), this equation states that there is a jump in the radial component of the magnetic field, H_ρ, due to the effect of the armour on H_ϕ and H_z.

The components of $\mathbf{H}$ can be expanded as in (8). With this setting, it can be shown [1] that Ampère's law in (14) leads to the same constraints (10) and (11) for the terms of $\mathbf{H}$, i.e.

$$H_m^\phi(\rho) = \frac{p_c}{2\pi\rho} H_m^z(\rho) \quad \text{and} \quad H_m^\rho(\rho) = \frac{p_c}{j2\pi m}(H_m^z)'(\rho), \tag{22}$$

where $H_m^z(\rho)$ is to be determined. The application of (22) to (21) yields the following equation for terms H_m^z:

$$\chi_\rho\Big[(H_m^z)'(r_a + t/2) - (H_m^z)'(r_a - t/2)\Big] = t\eta_m^2 \chi_{\mathrm{eff}} H_m^z(r_a), \tag{23}$$

where [1]

$$\chi_{\mathrm{eff}} = \frac{\chi_{\phi\phi}}{K_c^2} + \frac{2\chi_{\phi z}}{K_c} + \chi_{zz}, \tag{24}$$

with $K_c = 2\pi r_a/p_c$. It must be observed that the procedure in [1] implicitly omits χ_ρ in (23). We infer then that the following approximation was made (as recently confirmed in [4]):

$$\chi_\rho \approx 1, \tag{25}$$

which means *neglecting the effect of the eddy currents on the radial component of the field*. As a consequence, *the radial component of the magnetic field, H_ρ, will not contribute to the power losses.*

The cylindrical approximation simplifies also the calculation of the total magnetic field. *Outside* of the armour the field is solenoidal: $\nabla \cdot \mathbf{H} = 0$. By combining this equation with (22), we obtain the modified Bessel equation for H_m^z

$$\rho^2 (H_m^z)'' + \rho (H_z^m)' - (\eta_m^2 \rho^2 + m^2) H_m^z = 0, \tag{26}$$

whose solution can be written, using (18), as

$$H_m^z(\rho) = \begin{cases} a_m I_m(\eta_m \rho) + H_{0_m}^z(\rho) & 0 \le \rho < r_a, \\ b_m K_m(\eta_m \rho) + H_{0_m}^z(\rho) & r_a \le \rho, \end{cases} \tag{27}$$

a_m and b_m being the integration constants. Observing that H_z is continuous on the cylinder's surface, with (18) and (25) in (23) we obtain the following value for H_m^z *in the armour*:

$$H_m^z(r_a) = -\frac{H_{0_m}^z(r_a)}{1 + \frac{\tau_m}{t\eta_m \chi_{\text{eff}}}} \frac{K_m(\eta_m \rho)}{K_m(\eta_m r_a)} + H_{0_m}^z(\rho), \tag{28}$$

where $\tau_m = I_m'(\eta_m r_a)/I_m(\eta_m r_a) - K_m'(\eta_m r_a)/K_m(\eta_m r_a)$.

Eventually, the cylindrical approximation is used to rewrite the expression of the power losses, (7), as

$$\Delta S = \frac{j\omega}{2} \int_0^{2\pi} \int_{r_{a-\frac{t}{2}}}^{r_{a+\frac{t}{2}}} \mu_0 \mathbf{M} \cdot \mathbf{H}_0^* \mathrm{d}\phi \mathrm{d}\rho, \tag{29}$$

where note that the integration is over the cross section of the armour to give the losses per unit length. Using (15), (6), (23), (25), and (28), we can perform the above integration to obtain:

$$\Delta S = \frac{j\omega}{2} \mu_0 N l_a \pi r_w^2 \sum_{m=3k+1,\, k\in\mathbb{Z}} \chi_{\text{eff}} H_m^z(r_a) H_{0_m}^{z^*}(r_a). \tag{30}$$

4 Susceptibilities

The last missing piece for computing the power losses with (30) is an expression for the susceptibilities $\chi_\perp$ and $\chi_\parallel$. In the *local system*, each susceptibility acts independently from the other, as indicated by (13). It is therefore in this system that the susceptibilities are derived. Here, the armour appears as shown in Fig. 3. We can realize this by positioning ourselves on a wire, and then moving towards the direction indicated by $\mathbf{u}_\perp$: the armour appears as an *infinite* set of *parallel straight* wires. This is the same perspective adopted by [1, 4].

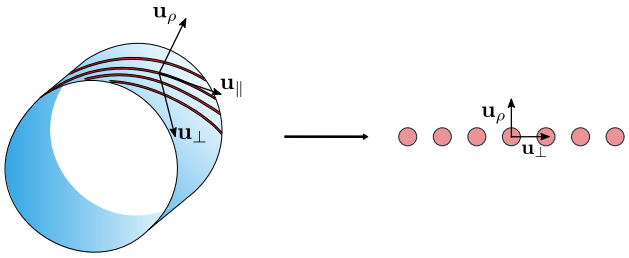

Fig. 3 Appearance of the armour in the local system (on the right)

The susceptibilities must be suitably *defined* to incorporate the effect of eddy currents. The TB adopts an energetic perspective for the definition. The idea is to leverage the cylindrical approximation in Fig. 2 by replacing the armour with a cylindrical sheet whose equivalent susceptibilities reproduce the active and reactive power of the actual armour in an external magnetic field [4]. Such a definition yields the following expressions for the susceptibilities, upon solving problem (12) for the configuration of Fig. 3 [1, 4]:

$$\chi_\perp = \frac{2}{\frac{\mu_r + \kappa r_w s_1}{\mu_r - \kappa r_w s_1} - \tau_{11} r_w^2}, \tag{31}$$

$$\chi_\parallel = \frac{2\mu_r}{\kappa r_w} \frac{I_1(\kappa r_w)}{I_0(\kappa r_w)} - 1, \tag{32}$$

where $\kappa = \sqrt{j\omega\mu_0\mu_r\sigma}$, $\tau_{11} = \frac{1}{3}(N l_a/2r_a)^2$, and $s_1 = I_1'(\kappa r_w)/I_1(\kappa r_w)$.

5 Test up to 15 kHz and discussion

This section presents a test on a model cable up to 15 kHz, which extends those published in [1, 4]. The losses are calculated with three different approaches:

- a FEM calculation [7];
- an integral numerical formulation based on the method of moments (MoM) [8];
- the analytical formulae proposed by the TB [1].

The parameters of the model cable are listed in Table 1.

The cable is tested in contralay configuration, which requires that $p_a p_c > 0$, whereas for equilay one would need $p_a p_c < 0$: this rather uncommon convention is a consequence of the definition of θ in (1), and of writing term $2\pi z/p_c$ with a positive sign in the exponential in (8). For

Table 1 Cable model parameters

Parameter	Symbol	Value
Rated current	I_c	$800\sqrt{2}$ A
Number of armour wires	N	95
Armour helix radius	r_a	113.31 mm
Armour helix pitch	p_a	2000.0 mm
Wire radius	r_w	3.5 mm
Wire relative permeability	μ_r	$300\, e^{-j\pi/3}$
Conductors helix radius	r_c	56.961 mm
Conductors helix pitch	p_c	3000.0 mm
Conductivity	σ	$4.8077 \cdot 10^6$ S/m
Frequency	f	50 Hz

example, with negative p_a and p_c conductors and wires are wound as in Fig. 1, which shows a contralay configuration.

The FEM approach is the one making the least number of approximations on the quasi-magnetostatic model (12), hence it is taken as the reference. Figure 4 shows a detail of the mesh used to model the armour wires. In order to model the eddy currents' distribution in the wires, it was considered that the skin depth is, using the data in Table 1, $\delta = \frac{1}{\sqrt{\pi f \sigma |\mu_0 \mu_r|}} \approx 1.08 \cdot 10^{-4}$ m at 15 kHz. Using this datum, eight circular layers were built starting from the boundary of each armour wire: the first layer has a thickness of $5 \cdot 10^{-5}$ m, which is approximately half of the skin depth; the thickness of the following layers was increased following a geometric progression with ratio 1.2. The 8th layer, in particular, has a thickness of $1.79 \cdot 10^{-4}$ m, which is approximately $1.66\,\delta$. The total thickness of the eight circular layers is

$$\sum_{k=0}^{7} 5 \cdot 10^{-5} \cdot 1.2^k \approx 8.25 \cdot 10^{-4} \approx 7.34\,\delta, \tag{33}$$

which, considering that eddy currents completely decay at a distance of $(4 \div 5)\delta$ from the boundary, is thick enough to model the skin effect up to 15 kHz. The mesh was then the same at all frequencies. The eddy current density induced in some armour wires at different frequencies computed by FEM is represented in Fig. 5, 6 and 7. It was verified that using six instead of eight layers did not change numerical results, showing that with eight layers the convergence is reached.

The total length of the simulated cable was three times the cross-pitch, whose absolute value is $\left|\frac{1}{p_c} - \frac{1}{p_a}\right|^{-1} = 6$ m. This allows to divide the cable into three sections: the two extreme sections are used to mitigate the boundary effects arising from the truncation of the geometry, while the central section is used to compute the losses per unit length. Eventually, quadratic elements were used to approximate the fields' and currents' distribution in the cable, and the total mesh has $\sim 10^8$ degrees of freedom. Magnetic insulation conditions are imposed at the boundaries of the computational domain.

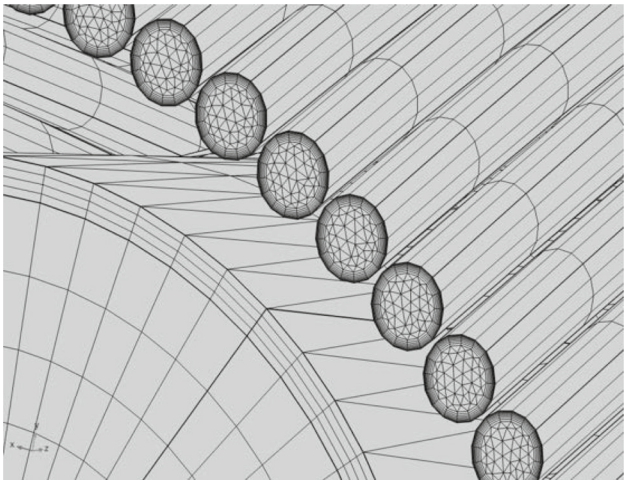

Fig. 4 Current density distribution $[A/\text{mm}^2]$ in the armour wires at 50 Hz

Figure 8 compares the losses calculated with all the available approaches. The results are all in good agreement with each other, but it is possible to spot some gaps between the curves.

A first test has been performed, in which the frequency is fixed at 50 Hz and the number of armour wires is gradually increased from 1 to 95. The cable is tested both in contralay and equilay configurations. The losses are calculated with the three available approaches, namely FEM, MoM, and TB formulae. The results are depicted in Fig. 9, and show good agreement between all approaches both in the contralay and equilay configurations.

Taking then the FEM curve as the reference, it is possible to compute the *absolute* discrepancy between the FEM losses and the other two approaches as

$$\Delta_{\text{MoM}} = |\text{MoM} - \text{FEM}| \quad \text{and} \quad \Delta_{\text{TB}} = |\text{TB} - \text{FEM}|, \tag{34}$$

which are plotted against frequency in Fig. 10.

In order to discuss the curves of Fig. 10, it is useful to outline the main features of the MoM approach, which shares some common approximations with the TB. The MoM formulation divides each wire in a finite number of cylinders, and it exploits the approximation in (16) to assume that the magnetization in each cylinder is uniform. The height of the cylinders is fixed and set equal to the diameter of the armour wires: for the cable under test the height is 7 mm (see Table 1). The magnetic field in the i-th armour wire is computed starting from the Biot–Savart law which, under the

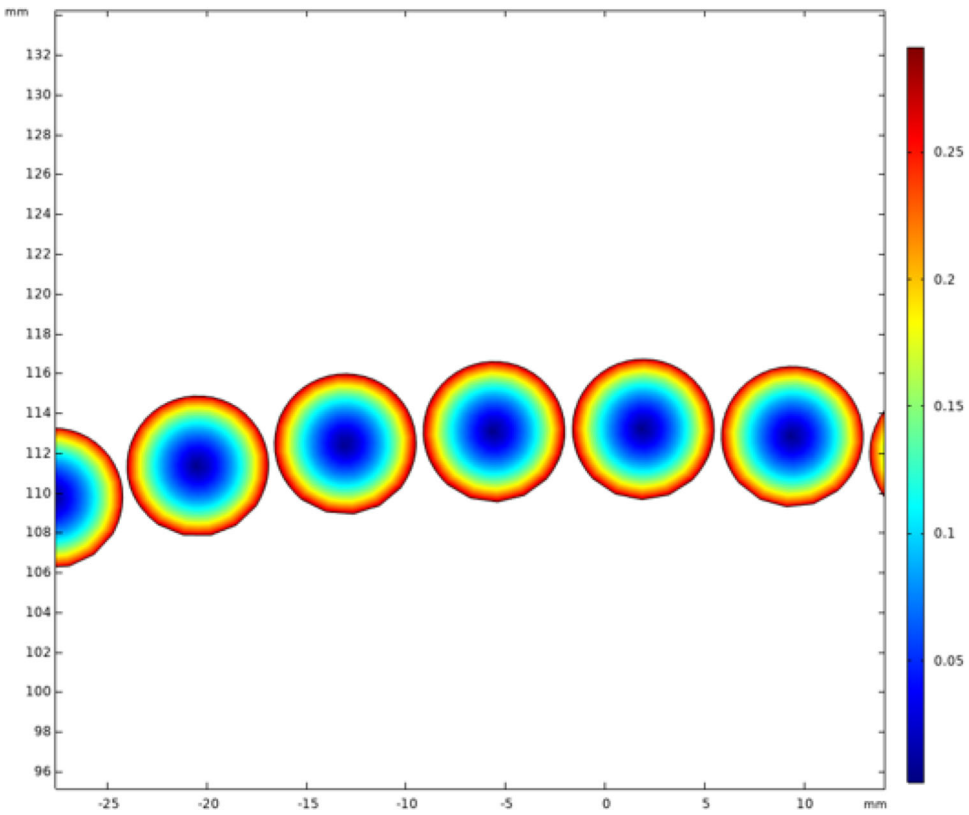

Fig. 5 Current density distribution $[A/\text{mm}^2]$ in the armour wires at 1 KHz

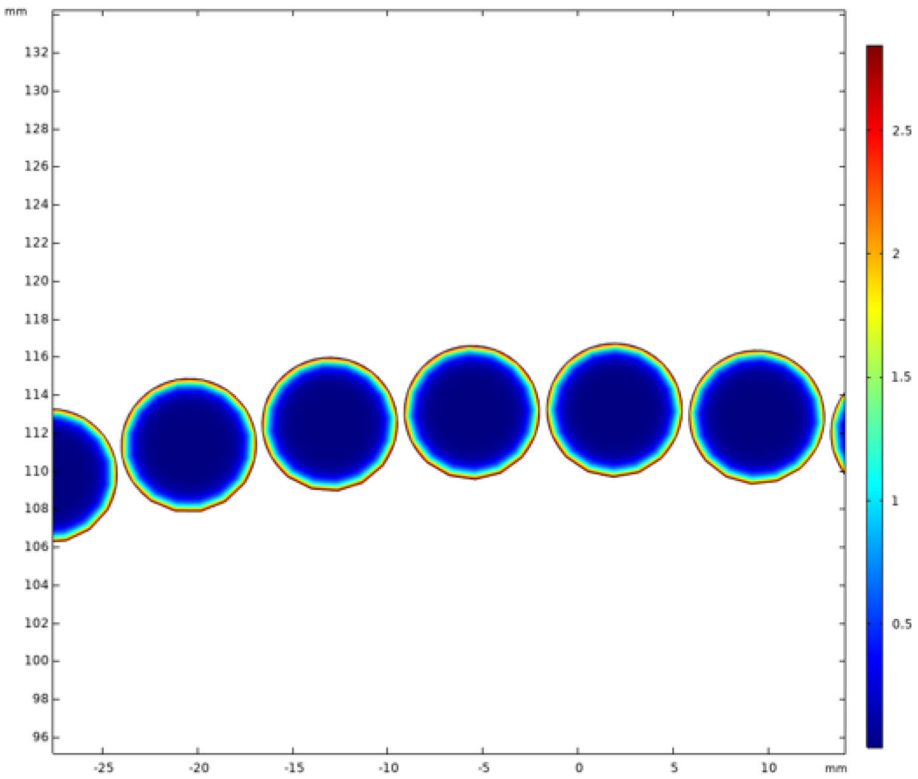

Fig. 6 Current density distribution $[A/\text{mm}^2]$ in the armour wires at 15 KHz

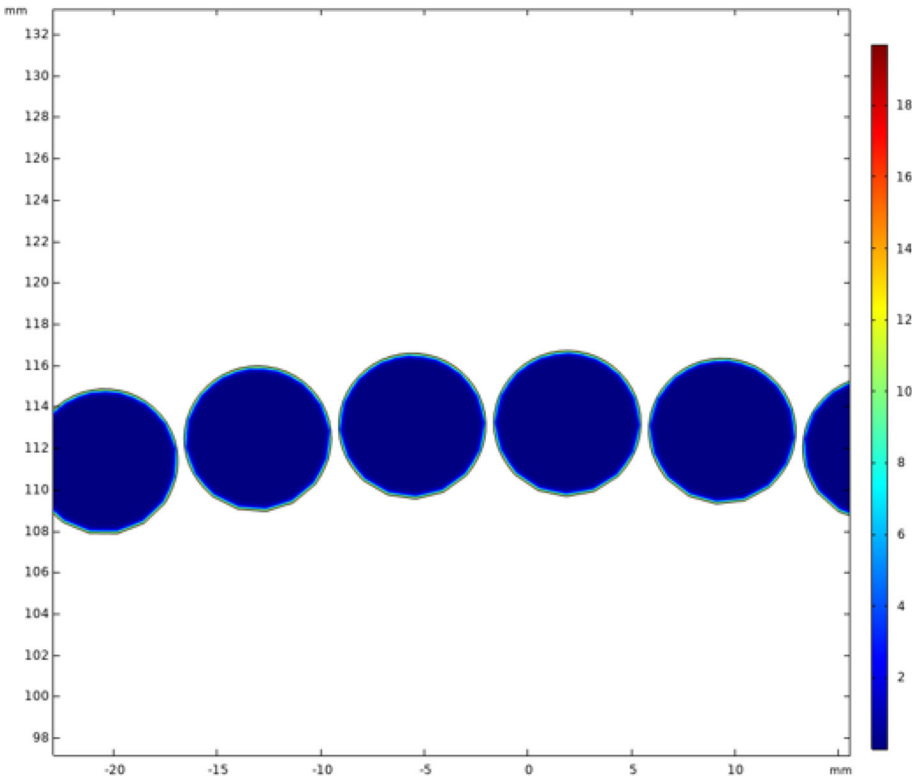

Fig. 7 Armour losses vs. number of armour wires, $f = 50\,\text{Hz}$, $T = 20\,^{\circ}\text{C}$. The plot is in linear vs. log scale

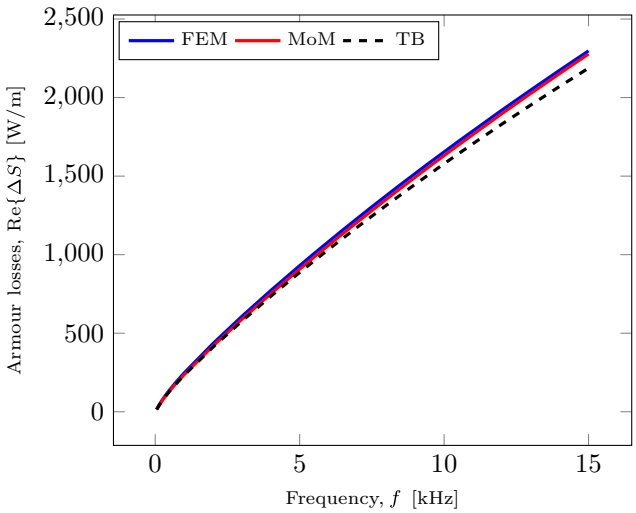

Fig. 8 Detail of the FEM mesh used to model the armour wires

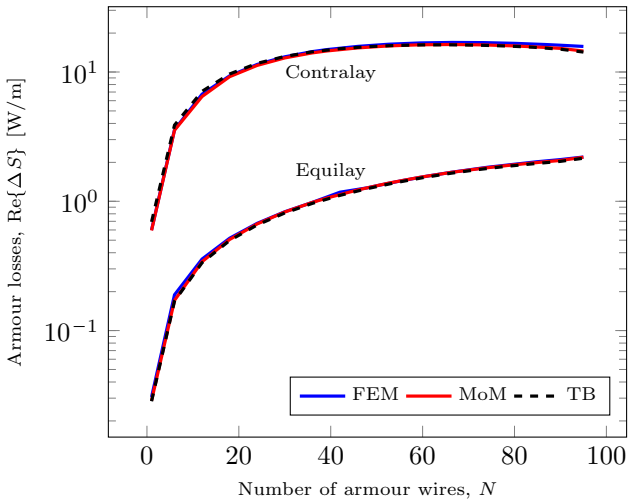

Fig. 9 Armour losses vs. frequency

assumption of uniformity in the cylinders [8], reads

$$\mathbf{B}_i(\mathbf{x}) = -\frac{\mu_0}{4\pi}\sum_j\sum_{k_j}\int_{S_{k_j}} \mathbf{n}\times\mathbf{M}(\mathbf{x}')\frac{\mathbf{x}-\mathbf{x}'}{|\mathbf{x}-\mathbf{x}'|^3}d^2x', \quad (35)$$

where j is an index for the wires (including the i-th), while k_j identifies a cylinder in the j-th wire and S_{k_j} is the boundary of such a cylinder. Vector $\mathbf{M}$ is the uniform magnetization in the cylinder. Of course, the magnetization must change from one cylinder to the other. In order to account for the induced eddy currents and magnetization, the MoM formulation considers two equivalent susceptibilities, $\chi'_\perp$ and $\chi'_\parallel$, which are given by [8, 13]:

$$\chi'_\perp = \frac{1}{\kappa r_w}\frac{J_1(\kappa r_w)}{J'_1(\kappa r_w)} - 1, \quad (36)$$

$$\chi'_\parallel = \chi_\parallel, \quad (37)$$

where J_1 is the first-order Bessel function. Please note that both the TB and the MoM approaches introduce parallel and perpendicular magnetic susceptibilities, even if they have different expressions in the two models in the perpendicular case.

Expression (36) was originally derived by Igarashi [13], who considered a *single* wire immersed in an orthogonal background field: the TB, on the other hand, derives $\chi_\perp$ *for the entire armour*, accounting for the mutual influence between the wires. In the numerical formulation, the combined effect of the wires is later taken into account by modelling the actual three-dimensional geometry of the armour.

Susceptibility $\chi'_\parallel$ is explicitly derived in [8] by considering the magnetization and the eddy currents induced in a single wire for a uniform background field along $\mathbf{u}_\parallel$. On the other hand, as observed in [4], the wires immersed in a parallel field do not affect each other, thus the approach adopted by the TB must yield the same result for $\chi_\parallel$. The MoM formulation, eventually, relies on the following susceptibility tensor, which applies *to a single wire*:

$$\chi_m^{\ell\,\prime} = \mathrm{diag}\left(\chi'_\perp, \chi'_\perp, \chi'_\parallel\right). \tag{38}$$

Note the difference in the first diagonal term between (38) and (13): in the MoM formulation the radial and perpendicular directions are identical.

Summarizing, the MoM formulation and the TB both start from the approximation in (16) to tackle the problem in two different ways: while the MoM formulation retains the 3D description of the geometry, the TB takes one step further to reach a full 2D model.

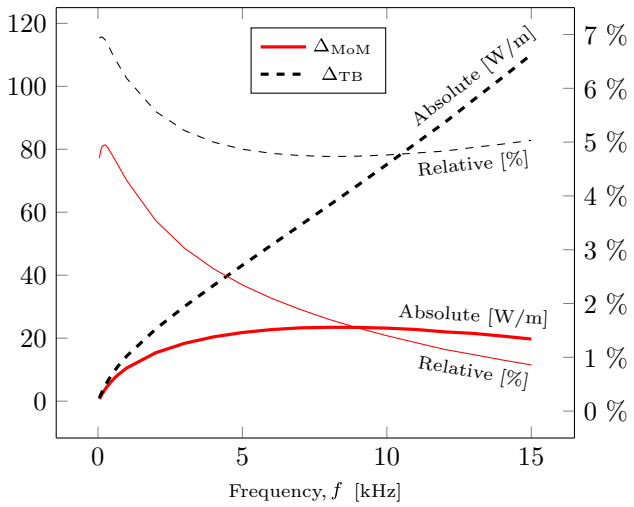

Fig. 10 Discrepancy vs. frequency. The relative discrepancies are obtained dividing the expressions in (34) by the FEM losses

Looking at the *absolute* curves in Fig. 10, one can see that the MoM curve is initially increasing, then reaches a maximum between 10 kHz and 15 kHz and begins to decrease. Although it is not possible to infer anything for the trend beyond 15 kHz, the result indicates that in the tested frequency range the discrepancy between the MoM approach and the FEM approach is limited. On the other hand, the *absolute* TB curve shows a linear increase of the discrepancy with FEM starting between 0 and 5 kHz, and such a trend is maintained up to 15 kHz.

Looking now at the *relative* curves in Fig. 10, we can see that the MoM curve has an initial peak and after that it decreases monotonically up to 15 kHz. The TB curve has an initial peak as well, then has a minimum between 5 kHz and 10 kHz and starts to rise. The MoM curve is always below 5 %, while the TB curve is always below 7 %: this shows a similar accuracy of the two approaches. Armour losses represent a minor fraction of the total losses in a three-core cable: about $10-12\%$ in contralay stranding, $4-5\%$ in equilay stranding. For this reason, the level of accuracy of TB formulas and MoM is adequate for practical system engineering applications.

Another interesting aspect to observe concerns the approximation on $\chi_\perp$ proposed by the TB:

$$\chi_\perp \approx \frac{2}{1-\tau_{11}r_w^2} \quad \text{when } |\mu_r| \gg 1. \tag{39}$$

Looking at (31), this means deeming term $\kappa r_w s_1$ as negligible when compared to μ_r. Indeed, for large $|\mu_r|$ it is possible to show that

$$|\kappa r_w s_1| \sim |\kappa r_w| \propto \sqrt{|\mu_r|} \ll |\mu_r|. \tag{40}$$

On the other hand, the approximated expression of $\chi_\perp$ is left with coefficient $\tau_{11}r_w^2$ only, which depends just on the geometric parameters of the cable. The plot in Fig. 11 compares the armour losses calculated using FEM, and using the TB's formulae without and with the approximation in (39): adopting the approximated expression for the susceptibility significantly worsens the estimate of the power losses at frequencies above 50 Hz.

6 Conclusion

This paper investigated the accuracy of the analytical formulae derived in the CIGRE Technical Brochure 908 [1] concerning the calculation of the power losses in the armour of single-armoured tripolar AC cables from 50 Hz to 15 kHz, extending the tests of the TB which considered only 50 Hz.

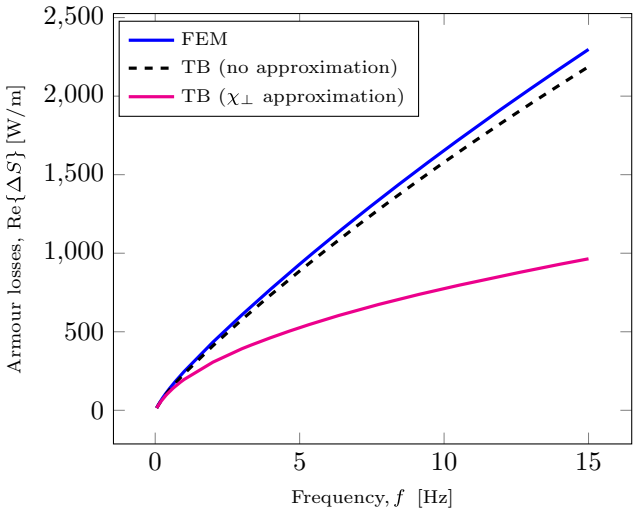

Fig. 11 Armour losses vs. frequency, $T = 20\,^{\circ}\mathrm{C}$, $N = 95$

Section 3 reviewed the implications arising from the cylindrical approximation depicted in Fig. 2, showing in detail how the solution of (14) is simplified.

Section 5 discussed the behaviour of the analytical formulae with respect to frequency. It showed that the TB formulae can provide reasonable estimates of the power losses up to 15 kHz on a typical cable, but their error increases linearly with frequency. Moreover, it was shown that using the approximation in (39) for $\chi_\perp$ significantly worsens the calculation of the power losses at frequencies above 50 Hz.

In conclusion, this work extended the tests of the CIGRE Technical Brochure 908 by probing the proposed analytical formulae up to 15 kHz: this can be useful in view of the necessity of evaluating the performance of cables in the presence of high-order harmonics generated by power converters connected to the grid.

Appendix A: Proof of the starting formula for ΔS

This appendix demonstrates the validity of equation (3), which is the starting point used by the TB to compute the power losses.

First of all, in the time-harmonic regime with complex-valued vector fields, let us define ΔS as the variation of power *in the entire space*,

$$\Delta S = \frac{\mathrm{j}\omega}{2} \int_{V_a \cup V_a^c} (\mathbf{B} \cdot \mathbf{H}^* - \mathbf{B}_0 \cdot \mathbf{H}_0^*) \mathrm{d}v, \tag{A1}$$

where V_a is armour volume and V_a^c is the complementary region in $\mathbb{R}^3$, i.e. the air volume. Through the following algebraic manipulation, we find that:

$$\begin{aligned}\mathbf{B} \cdot \mathbf{H}^* - \mathbf{B}_0 \cdot \mathbf{H}_0^* &= \mathbf{B} \cdot \mathbf{H}^* - \mathbf{B}_0 \cdot \mathbf{H}_0^* \\ &+ \mathbf{B} \cdot \mathbf{H}_0^* - \mathbf{B} \cdot \mathbf{H}_0^* + \mathbf{H} \cdot \mathbf{B}_0^* - \mathbf{H} \cdot \mathbf{B}_0^* \\ &= (\mathbf{B} \cdot \mathbf{H}_0^* - \mathbf{H} \cdot \mathbf{B}_0^*) + \mathbf{B} \cdot (\mathbf{H}^* - \mathbf{H}_0^*) + \mathbf{B}_0^* \cdot (\mathbf{H} - \mathbf{H}_0).\end{aligned}$$

Therefore, (A1) can be rewritten as

$$\begin{aligned}\Delta S = \frac{\mathrm{j}\omega}{2} \int_{V_a \cup V_a^c} (\mathbf{B} \cdot \mathbf{H}_0^* - \mathbf{H} \cdot \mathbf{B}_0^*) \mathrm{d}v + \frac{\mathrm{j}\omega}{2} \\ \int_{V_a \cup V_a^c} \mathbf{B} \cdot (\mathbf{H}^* - \mathbf{H}_0^*) \mathrm{d}v + \frac{\mathrm{j}\omega}{2} \int_{V_a \cup V_a^c} \mathbf{B}_0^* \cdot (\mathbf{H} - \mathbf{H}_0) \mathrm{d}v.\end{aligned} \tag{A2}$$

Now we exploit a theorem demonstrated in [14], which states that given two vector fields $\mathbf{P}$ and $\mathbf{Q}$ such that

$$\nabla \times \mathbf{P} = 0, \qquad \nabla \cdot \mathbf{Q} = 0, \tag{A3}$$

$$\lim_{\rho \to \infty} \rho \mathbf{P} = \mathbf{0}, \qquad \lim_{\rho \to \infty} \rho \mathbf{Q} = \mathbf{0}, \tag{A4}$$

then

$$\int_{\mathbb{R}^3} \mathbf{P} \cdot \mathbf{Q} \mathrm{d}v = 0. \tag{A5}$$

For the problem at stake, we have that

$$\nabla \cdot \mathbf{B} = \nabla \cdot \mathbf{B}_0 = 0, \tag{A6}$$

thus we let

$$\mathbf{Q} = \mathbf{B} \quad \text{and} \quad \mathbf{Q}_0 = \mathbf{B}_0. \tag{A7}$$

Then, being $\mathbf{J}$ the current density of the phase conductors,

$$\nabla \times \mathbf{H} = \nabla \times \mathbf{H}_0 = \mathbf{J} \implies \nabla \times (\mathbf{H} - \mathbf{H}_0) = 0 \tag{A8}$$

and we let

$$\mathbf{P} = \mathbf{H} - \mathbf{H}_0. \tag{A9}$$

It is important to stress that (A8) holds as long as $\mathbf{J}$ is only the current of the phase conductors: this holds if the complex susceptibility that binds $\mathbf{B}$ and $\mathbf{H}$ incorporates the conductive effects, which is indeed the approach followed by the TB and this paper.

It can be shown, [12], that $\mathbf{B}_0$ and $\mathbf{H}_0$, the fields generated by the phase wires without the armour, decay as $e^{-\rho}/\sqrt{\rho}$ as $\rho \to \infty$. Fields $\mathbf{B}$ and $\mathbf{H}$, that are calculated in presence the armour, decay even faster. Thus, the asymptotic conditions in (A4) required by the theorem for fields $\mathbf{Q}$, $\mathbf{Q}_0$, and $\mathbf{P}$ defined in (A7) and (A9) are satisfied.

Using then (A5), we have that

$$\int_{V_a \cup V_a^c} \mathbf{B} \cdot (\mathbf{H}^* - \mathbf{H}_0^*) \mathrm{d}v = \int_{V_a \cup V_a^c} \mathbf{Q} \cdot \mathbf{P}^* \mathrm{d}v = 0, \quad \text{(A10)}$$

$$\int_{V_a \cup V_a^c} \mathbf{B}_0^* \cdot (\mathbf{H} - \mathbf{H}_0) \mathrm{d}v = \int_{V_a \cup V_a^c} \mathbf{Q}_0^* \cdot \mathbf{P} \mathrm{d}v = 0, \quad \text{(A11)}$$

and

$$\Delta S = \frac{\mathrm{j}\omega}{2} \left[\int_{V_a} (\mathbf{B} \cdot \mathbf{H}_0^* - \mathbf{H} \cdot \mathbf{B}_0^*) \mathrm{d}v + \int_{V_a^c} (\mathbf{B} \cdot \mathbf{H}_0^* - \mathbf{H} \cdot \mathbf{B}_0^*) \mathrm{d}v \right]. \quad \text{(A12)}$$

In air $\mathbf{B} = \mu_0 \mathbf{H}$ and $\mathbf{B}_0 = \mu_0 \mathbf{H}_0$, thus

$$\int_{V_a^c} (\mathbf{B} \cdot \mathbf{H}_0^* - \mathbf{H} \cdot \mathbf{B}_0^*) \mathrm{d}v = 0, \quad \text{(A13)}$$

and we conclude that the power variation is

$$\Delta S = \frac{\mathrm{j}\omega}{2} \int_{V_a} (\mathbf{B} \cdot \mathbf{H}_0^* - \mathbf{H} \cdot \mathbf{B}_0^*) \mathrm{d}v, \quad \text{(A14)}$$

which is indeed (3).

Author Contributions P. Cambareri wrote the main manuscript text. All authors reviewed the manuscript.

Funding Open access funding provided by Politecnico di Milano within the CRUI-CARE Agreement.

Data Availability No datasets were generated or analysed during the current study.

Declarations

Conflict of interest The authors declare no conflict of interest.

References

1. Losses in armoured three core power cables, CIGRE Technical Brochure 908, Working Group WG B1.64. Publisher: Conseil International des Grands Réseaux Électriques (CIGRE), Paris, France, (2023)
2. Electric cables "Calculation of the current rating - Part 1-1: Current rating equations (100 % load factor) and calculation of losses" General, IEC Standard 60287-1-1, Technical Committee TC 20 - Electric Cables. Publisher: International Electrotechnical Commission, Geneva, Switzerland, (2014)
3. Hatlo M, Olsen E, Stølan R, Karlstrand J (2015) "Accurate analytic formula for calculation of losses in three-core submarine cables", Jicable '15 (9th International conference on insulated power cables), Versailles, France, June 2015
4. Hatlo M, Hovde M (2024) "Analytical formula for calculation of armour losses in three-core power cables," arXiv preprint arXiv:2404.06998
5. Goddard KF, Pilgrim JA, Chippendale R, Lewin PL (2015) Induced losses in three-core SL-type high-voltage cables. IEEE Trans Power Delivery 30(3):1505–1513
6. Bakhshizadeh MK, et al (2016) "Harmonic modelling, propagation and mitigation for large wind power plants connected via long HVAC cables: Review and outlook of current research," IEEE International Energy Conference (ENERGYCON), Leuven, Belgium, pp. 1-5, https://doi.org/10.1109/ENERGYCON.2016.7513982
7. COMSOL Multiphysics® v. 6.2. COMSOL AB, Stockholm, Sweden. www.comsol.com
8. Giussani L, Bechis M, de Falco C, Di Rienzo L (2018) An integral formulation for an array of wires in a 3-D magneto-quasi-static field. IEEE Trans Magn 54(7):1–8
9. Giussani L, Di Rienzo L, Bechis M, de Falco C (2021) Computation of armor losses in AC submarine cables. IEEE Trans Power Deliv 36(5):3014–302
10. Giussani L, Di Rienzo L, Bechis M, de Falco C (2022) Fully coupled computation of losses in metallic sheaths and armor of AC submarine cables. IEEE Trans Power Deliv 37(5):3803–3812
11. Jackson JD (1975) Classical electrodynamics, 2nd edn. John Wiley and Sons, New York, NY, USA, p 216
12. Haber F (1974) "The magnetic field in the vicinity of parallel and twisted three-wire cable carrying balanced three-phased currents," in IEEE transactions on electromagnetic compatibility, vol. EMC-16, (6), pp. 76–82
13. Igarashi H (2017) Semi-analytical approach for finite-element analysis of multi-turn coil considering skin and proximity effects. IEEE Trans Magn 53(1):7400107
14. Stratton JA (1941) Electromagnetic theory, 1st ed., pp. 111–112. McGraw-Hill Book Company: New York